

Resonant photoemission at the absorption edge of Mn and Ti and electronic structure of 1T-Mn_{0.2}TiSe₂

M.V. Yablonskikh^{a,*}, A.S. Shkvarin^b, Y.M. Yarmoshenko^b, N.A. Skorikov^b,
A.N. Titov^{b,c}

^a*Sincrotrone Trieste SCpA, Basovizza I-34012, Italy*

^b*Institute of Metal Physics, Russian Academy of Sciences-Ural Division, 620041
Yekaterinburg, Russia*

^c*Ural State University, pr. Lenina 51, Yekaterinburg, 620089 Russia*

Abstract

Resonant valence-band X-ray Photoemission Spectra (ResPES) excited at 2p_{3/2} core level energies, 2p_{3/2} X-ray Photoelectron Spectra (XPS) and L_{3,2} X-ray Absorption Spectra (XAS) of Ti and Mn in single crystal of 1T-Mn₂TiSe₂ were studied for the first time. The ionic-covalent character of bonds formed by Mn atoms with the neighboring Se atoms in the octahedral coordination is established. Atomic multiplet calculations of Ti and Mn L_{3,2} XAS and calculations of electronic structure of 1T-Mn_{1/8}TiSe₂ compound were performed. It is found that Ti atoms are in ionic state of 4+ and Mn atoms are in the state of 2+. In ResPES of Mn_{0.2}TiSe₂ excited near Ti and Mn 2p_{3/2} absorption edges narrow Ti 3d and Mn 3d bands at energies just below the Fermi level are observed. According to band structure calculations E(**k**) Ti 3d states are localized in the vicinity of Γ point and Mn 3d states are localized along the direction M- Γ -K in the Brillouin zone of the crystal.

Keywords:

PACS: 74.25.Jb, Electronic structure

PACS: 31.10.+z, Theory of electronic structure, electronic transitions, and chemical bonding

PACS: 71.20.Be, Transition metals and alloys

PACS: 78.70.Dm, X-ray absorption spectra

PACS: 79.60.-i, Photoemission and photoelectron spectra

*Corresponding author.

Email address: mikhail.yablonskikh@gmail.com (M.V. Yablonskikh)

1. Introduction

Layered dichalcogenides of Ti intercalated with transition metals TM_xTiZ_2 (TM-transition metal, $\text{Z} = \text{S, Se, Te}$) show a promise in creation of monoatomic layers of magnetic metals with a set concentration. These layers are separated by nonmagnetic slabs of the TiZ_2 matrix. Such substances are natural analogs of nanostructures. The systematic studies [1, 2, 3] of chemical bonding in the M_xTiZ_2 compounds revealed that hybridization of 3d states of an interstitial metal atom and its nearest neighborhood is pure covalent in origin. Such feature of the chemical bonding manifests itself in a shrinking of the lattice in the direction aligned with the normal to the basis plane [4], decrease in conductivity [2], formation of narrow and dispersion-less bands in the vicinity of the Fermi level [5, 6], and suppression of the magnetic moment of interstitial atoms [7] due to delocalization of their 3d-electrons. The only exclusion from this group of materials is the Mn-TiSe₂ system which, upon intercalation, exhibits an increase in the interlayer spacing, growth of conductivity [8], and anomalously high (by the order of magnitude) increment of the Pauli contribution to the magnetic susceptibility in comparison with the other intercalated metals [9].

In our work experimental data were taken on single crystals of the $1\text{-Mn}_x\text{TiSe}_2$ ($x=0.1, 0.2$) compounds. To ascertain the reason for the anomalous behavior of the Mn-TiSe₂ system, X-ray Photoelectron Spectra (XPS) of the Ti 2p and Mn 2p core levels, $\text{L}_{3,2}$ X-ray Absorption Spectra XAS of Ti and Mn, and resonant valence-band photoemission (ResPES) have been investigated.

2. Experiment and calculations

Polycrystalline samples were synthesized from starting elements by the ampoule synthesis method. Powder diffractometry together with magnetic measurements showed a good quality of samples in accordance with the available literature data [7, 8, 10]. Single crystals of Mn_xTiSe_2 were grown by the gas-transport reaction technique with I_2 as a gas-carrier in evacuated quartz ampoules from a polycrystalline phase. Crystals have a form of thin plates of about $2 \times 1 \times 0.05 \text{ mm}^3$ in size. The chemical composition was determined by X-ray fluorescence analysis using a JEOL-733 spectrometer. The

crystal structure the same as reported on earlier [7]. The analysis showed the preservation of composition of the initial phase in the course of growing single crystals. A fragment of the crystal structure and the Brillouin zone of the compound $1\text{T-Mn}_x\text{TiSe}_2$ is shown in Fig. 1.

Spectroscopic measurements were performed at BACH beamline [11] of the Elettra synchrotron Facility. Photoelectron Spectra were taken using an VSW 150 photoelectron analyzer with the acceptance angle of 8 degrees. X-ray absorption data were measured in the Total Electron Yield (TEY) mode. The sample was cleaved in-situ in a vacuum $3\text{-}5 \cdot 10^{-10}$ Torr. XPS of the C 1s, O 1s and Ti 2p core levels were measured from time to time to check for a possible contamination of the surface during the measurements. The intensity of carbon and oxygen 1s peaks in survey spectra was extremely low and the shape of Ti 2p XPS remained unchanged during the measurement. The absence of the titanium oxide like satellite peaks in Ti 2p XPS ensures of the absence of oxidation at the sample surface and in the bulk. The angle between the incoming beam and the normal to the basis plane of the sample was 60 degrees. The normal to the sample coincides with the c axis which was aligned with the axis of the analyzer. Both the c -axis [001] of the sample and the polarization of the incident X-ray were in horizontal plane. The energy resolution of the monochromator i.e, the energy resolution of XAS of Ti 2p and Mn 2p was set to 0.1 eV. The photoelectron analyzer resolution was set to 0.147 eV. It results in the total energy resolution of 0.19 eV for XPS and ResPES. Binding and monochromator energy scales were calibrated through the binding energy of Au $4f_{3/2}$ level and through the Fermi edge measurements.

Band structure calculations were performed using the full-potential augmented plane-wave method as implemented in WIEN2k code [12]. To account for the exchange-correlation potential we employed the gradient approximation [13] in the Perdew-Burke-Ernzerhof variant. The Brillouin zone integrations were performed with a $7 \times 7 \times 3$ special \mathbf{k} - point grid and $R_{MT}^{min} \cdot K_{max} = 7$ (the product of the smallest of the atomic sphere radii R_{MT} and the plane wave cutoff parameter K_{max}) was used for the expansion of the basis set. The experimentally determined lattice parameters of $\text{Mn}_{0.145}\text{TiSe}_2$ ($a_0 = 3.5770 \text{ \AA}$, $c_0 = 6.1645 \text{ \AA}$) were taken. The spheres radii were chosen as $R_{Mn} = 2.46$, $R_{Ti} = 2.5$, $R_{Se} = 2.19$ a.u. in a way that that the corresponding spheres were near the mutual touch. To account for an intercalation of TiSe_2 by Mn atoms we constructed a $2a_0 \times 2a_0 \times 2c_0$ supercell in which for one from many non-equivalent selenium atoms the z -parameter was chosen as in

pristine TiSe_2 whereas for the second Se atom (placed near the Mn layer) the experimentally determined z -parameter was used. The resulting unit cell has the same symmetry as the initial unit cell of the TiSe_2 : space group P-3m1 (164), see also Fig. 1. According to the results of the calculations Mn 3d electrons are spin-polarized and the magnetic moment at Mn atoms reaches $3 \mu_B$, that is in a good agreement with previously reported calculations [1].

Ti atoms in the intercalated compound can be classified in two types further labelled as Ti1 and Ti2. In the intercalated compound the nearest neighborhood of atoms Ti2 is identical to that in the matrix of TiSe_2 and those of Ti1 atoms corresponds to the situation when Mn atoms randomly occupy some sites in the second coordination shell of Ti1 as shown in Fig. 1. The point group symmetry of titanium atoms in TiSe_2 is D_{3d} . The crystal field splits Ti 3d level into $A_{1g}(3z^2 - r^2)$, $E_g^\pi(x^2 - y^2, xy)$ and $E_g^\sigma(xz, yz)$ sublevels. As a result of intercalation the symmetry of Ti atoms is lowered to the C_{3v} point group for Ti1 atoms and C_s for Ti2. Taking into account that nearest neighborhood of Ti (chalcogenic octahedra) is not changed during intercalation and defects which lower the symmetry occur in a second coordination sphere of Ti2 atoms and in the further spheres of Ti1 atoms, the calculation results are given in terms of the D_{3d} group. Our cluster calculation are restricted to use distorted octahedral surrounding of investigated atom. For a comparison of results of cluster and band structure calculations please note following. The analogue of cubic t_{2g} states of octahedral surrounding are A_{1g} and E_g^π states of trigonal basis (lobes of corresponding orbitals do not point towards atoms of nearest neighborhood). The analogue of cubic E_g are E_g^σ states of trigonal basis (lobes of corresponding orbitals point towards atoms of nearest neighborhood).

Atomic multiplet calculations of $L_{3,2}$ XAS of Ti^{4+} and Mn^{2+} in the octahedral surrounding were performed using the program [14]. For a case of Ti $L_{3,2}$ XAS calculations the best agreement with the experiment is achieved with the following specified parameters: Slater integrals are decreased to 75% the calculated value, parameter of splitting in the crystal field 10Dq set 1.2 eV, the charge transfer parameter Δ set 3 eV. For the case of Mn $L_{3,2}$ XAS the crystal field splitting 10Dq set 0 eV, Slater integrals set 100% of the calculated value, the charge transfer parameter Δ set 3 eV. The same values of the parameters were used to calculate Mn 2p core level photoelectron spectrum.

Since Mn_xTiSe_2 compounds with concentrations $x \leq 0.25$ can be treated as ideally two-dimensional [8] our experimental results can be discussed

within an appropriate two-dimensional model. Without ordering in TM sublattice, the crystal structure of these compounds is considered as a hexagonal.

3. Experiment, Theory and Discussion

3.1. XPS

The results of measurements of Ti 2*p* XPS are shown in Fig. 2. The binding energy of the Ti 2*p*_{3/2} maximum for Mn_{0.2}TiSe₂ is about 455.5 eV for $x=0.1$ and 455.8 eV for $x=0.2$ while for compound TiSe₂ it is equal to 455.4 eV [15],[2]. Ti 2*p* core level peaks in the spectral multiplet of the intercalated compound are essentially broadened in comparison with that from pure TiSe₂ [2],[15]. This is a result of formation of two types of Ti atoms which occupy correspondingly two nonequivalent types of crystallographically different positions as described in the Sec. 2. Under the assumption that both theoretical and experimental spectra consist of two spectral contributions originating from Ti1 and Ti2 sites and that spectral contribution from Ti2 atoms (TiSe₂) will prevail over that from Ti1 atoms a fit of the experimental Ti 2*p* XPS of Mn_{*x*}TiSe₂ for concentrations $x=0.2$ and 0.1 was performed.

Although the fitted XPS shown in the Fig. 2 can not precisely reproduce the experimental spectra, a principal agreement between experimental XPS and the fits is achieved. As can be easily seen, there is a correlation between the weighted components of the fits of Ti 2*p* XPS and the concentration x of intercalated Mn. Initial weight ratio of Ti2/Ti1 contributions in Ti 2*p* XPS is 80/20 for $x=0.1$. It changes approximately to 55/45 for $x=0.2$, i.e. approximately of factor two which corresponds to the doubling of Mn concentration. For these reasons the appearance of the contribution from Ti1 atoms in Ti 2*p* XPS is a result of intercalation. The energy shift of magnitude around 1 eV between the Ti1 and Ti2 spectral weights maxima is to illustrate that intercalation of Mn even with small concentration greatly affects electronic structure of TiSe₂ host lattice.

It is to be noticed that 2*p* core level XPS of TM in TMDC's are most informative [2] about their physical properties and chemical bonding in TMDC's. Mn 2*p* photoelectron spectrum shown in Fig. 3 exhibits a satellite structures at around 6 eV higher than the peak energies of Mn 2*p*_{3/2} and Mn 2*p*_{1/2} core levels. Multiplet calculation of Mn 2*p* photoelectron spectrum of Mn 2+ shown in Fig. 3 exhibits the presence of satellites at the same energy from that of Mn 2*p*_{3/2} and 2*p*_{1/2} peaks. According to the calculation results both the main and the satellite peaks are formed mostly by mixing final states

$2p^5 3d^6 \underline{L}$ and $2p^5 3d^5$ correspondingly. The shape of Mn 2p XPS is very close to that observed $Mn_{1/4}TiS_2$ [16]. Calculation Mn 2p X-ray photoelectron spectra performed for $Mn_{1/4}TiS_2$ also demonstrates similar satellite structure [17]. This match between experimental and computational data of Mn intercalated diselenide and disulphide indicate that a charge transfer occurs between manganese atoms and the ligand atoms. According to calculations for diselenide charge-transfer energy $\Delta = 3$ and for disulfide $\Delta = 4$ [17]. These satellites were not observed by us in the 2p spectra of Cr, Fe, Co and Ni intercalated in $TiSe_2$ [2, 1], which indicates a negligible charge transfer. This factor dramatically distinguishes Mn-compounds from all other intercalated materials. In $Mn_{0.2}TiSe_2$ chemical bond of Mn with the surrounding only is partially ionic. Electrons are transferred from the manganese ions in the state Mn^{2+} to the conduction band formed by the $Ti 3d$ states.

3.2. XAS

Let us discuss the $Ti L_{3,2}$ and $Mn L_{3,2}$ XAS (4) measured in the same experimental conditions as XPS. The $Ti L_{3,2}$ XAS are different both in the spectral shape and peak positions from the spectrum of pure $TiSe_2$ which we reported earlier [18].

Introduction of Mn atoms in the Van der Waals gap of the $TiSe_2$ matrix leading to deformation of chalcogenic surrounding of Ti atoms and the charge transfer from Mn into the conduction band is the main reason for difference in peak shape and energy positions of Ti 2p absorption spectrum relatively to that of $TiSe_2$ [19]. The amplitude of the deformation caused by this distortion of chalcogen octahedra is described by the parameter $\varepsilon = (2zc_0)/a_0$, where c_0 and a_0 are the lattice constants, and z is the coordinate of Se atom in the unit cell. The intercalation of Mn to the composition $Mn_{0.2}TiSe_2$ results in the change of ε from 0.8655 in $TiSe_2$ to 0.8792 ($\Delta\varepsilon = 0.0137$) in $Mn_{0.2}TiSe_2$. It has to be noted that the amplitude of deformation $\Delta\varepsilon$ has a quite large magnitude for case of Mn_xTiSe_2 in comparison with the cases of intercalation of other metals. For example, introduction of Cr results in the quantity $\varepsilon = 0.8651$ ($\Delta\varepsilon = 0.0004$), which is by two orders of magnitude smaller than that for $Mn_{0.2}TiSe_2$. Such deformation should increase the splitting of the lower unfilled $Ti 3d_{z^2}$ -orbital from the rest of $Ti 3d$ states, increase the binding energy of $Ti d_{z^2}$ orbital [20, 21, 22, 23, 24], and, consequently, result in the partial filling of the electronic states in the vicinity of the Fermi level.

As can be seen from Fig. 4 calculations of $Ti L_{3,2}$ absorption spectrum taken for Ti^{4+} are in a good agreement with experimental data. In the

calculated spectrum the main maxima **A** and **B** correspond to the mass centers of the e_g and t_{2g} orbitals, though they are strongly mixed. The splitting into (antibonding) t_{2g} and e_g orbitals of Ti L_3 and Ti L_2 components of the multiplet in the calculated crystal field is equal to 1.2 eV (Fig. 4) per contra to the case of TiSe_2 where the splitting is equal to 1.8 eV. The calculated absorption spectrum of Mn in the oxidation state 2+ reproduces the shape and energy position of the main spectral maxima much better than that for Ti case, see Fig. 4. Energy splitting of t_{2g} and e_g orbitals is absent.

3.3. ResPES

It has been stated that a photoemission of d electrons from 3d metals and their compounds is strongly enhanced if the energy of the incident photon exceeds the binding energy of the core level upon excitation of np electrons ($n=2,3$) to an unfilled 3d state, resulting in a resonant emission [25, 26, 27, 28]. This effect is interpreted as a result of a consistent process under which an np electron in the initial state first is excited to an empty 3d level, thus forming an intermediate bound state ($np, 3d$). Because of the autoionization process the intermediate bound state can transform into a final state identical to that resulting from the direct photoemission. A resonance of 3d electrons takes place upon the interference of the direct channel of photoemission ($np^6 3d^n + h\nu \rightarrow np^6 3d^{n-1} e_f$) with the successive decay of the excited state of the Coster-Kronig type ($np^6 3d^{n+1} + h\nu \rightarrow np^5 3d^{n+1} \rightarrow np^6 3d^{n-1} e_f$). Resonance peaks in the valence band are superimposed on Auger $L_{2,3}M_{4,5}M_{4,5}$ peak. They arise at the 2p edge of absorption and can essentially overlap with the valence band.

Resonant Photoelectron Spectra (ResPES) of the valence band of $\text{Mn}_{0.2}\text{TiSe}_2$ taken near the Ti $2p_{3/2}$ and Mn $2p_{3/2}$ excitation energies (further labelled as Ti $2p_{3/2}$ and Mn $2p_{3/2}$ ResPES for a brevity) are shown in Fig. 5 and Fig. 6 respectively. For both elements in cases of pre-resonant excitation a small broad peak in the range of 0.1-0.4 eV is observed. Following the increase of the excitation energy, a standard Auger L_3VV spectrum of constant kinetic energy and resonance peaks in the vicinity of the Fermi level appear both in Ti $2p_{3/2}$ and Mn $2p_{3/2}$ ResPES. In the normal mode of the Raman scattering (known in the mentioned literature [25, 26, 27, 28] as RRAS) an energy position of the Auger signal in the binding energy scale does not change with the excitation energy until the latter reaches the spectral maximum of TM $2p_{3/2}$ X-ray absorption spectrum. Similar behaviour was studied in detail for cases of some 3d metals in Ref. [29] where it was established that the

appearance of crossover peak which represents a transition from the RRAS to Auger mode is an element dependent, i.e. appears at different energy relatively to that of 2p absorption edge of Cr, Fe, and Ni. In our experiments the appearance of the crossover peak in resonant Ti 2p_{3/2} ResPES is occurred when the excitation energy reaches a spectral maximum of Ti L₃ absorption spectrum (label **f**) in Fig.5). Auger peak shown by down-arrows in Fig-s 5,6 changes the position in the binding energy scale in a way described above as. Important is that Auger contribution does not overlap with the part of the valence band near the Fermi energy. Near the Fermi energy an intensive resonance at the binding energy of Ti_d peak and small resonance at the energy of Mn_d peak are observed in Ti 2p and Mn 2p ResPES respectively.

At the final state of photoemission, a vacancy at the core level is absent. Since the influence of a hole in the valence band on a valence band spectrum is insignificant for case of 3d transition metals photoemission it is reasonable to compare calculated DOS and $E(\mathbf{k})$ calculations shown in Fig-s. 7,8 with valence band spectra shown in Fig-s 5,6. However, it needs to be said that a precise match between theory and experiment is not to be expected due to following reasons. At energies of excitation in the ranges of 2p resonance of Ti and Mn the electron inelastic mean free path does not exceed 10 Å [30]. Taking into account the magnitude of lattice constant equal to 6.15 for $x=0.2$ respectively, we estimate that the nearest to the crystal surface Van der Waals gap containing Mn atoms is located at a distance of around 12 Å). The distance is really close to the limits of electron inelastic mean free paths [30]. Besides, the crystal surface may lose a part of Mn atoms during the cleavage. Those are some important experimental limitations. Correct computational data are also to be provided only for certain concentrations for which a correct modeling is possible, see Sec. 2. Nevertheless, a good match achieved between the theory and experiment allows us to make a reasonable comparison.

According to the theoretical calculations of $E(\mathbf{k})$ in the vicinity of this point just below the Fermi level, the Ti 3d states are prevail (Figure 7). The Mn 3d states are localized mainly near the points k and M of the Brillouin zone (Figure7). There is a difference in localization character of Ti and Mn states in the calculated Brillouin zone shown in Fig. 7). According to the theoretical calculations of $E(\mathbf{k})$ in the vicinity of this point immediately under the Fermi level, the Ti 3d states prevail. The Mn 3d states are localized mainly near the points K and M of the Brillouin zone (7). During the measurements the sample was oriented in a way that c- axis of the crystal is

parallel to the analyzers axis. This experimental geometry creates a favorable conditions for electron emission from the vicinity of in Γ point for the crystal of $\text{Mn}_{0.2}\text{TiSe}_2$ in this experimental geometry. Although photoionization cross-section of Ti 3d is approximately 3-4 times as large as that for Mn 3d [31] at the energy of corresponding 2p threshold, the sample orientation may cause the intensity of Ti_d resonant peak in Ti 2p ResPES in $\text{Mn}_{0.2}\text{TiSe}_2$ to be significantly larger than that of Mn_d peak in Mn 2p ResPES, where intensities are estimated relatively to the rest of the manifold.

In the calculated local density of 3d states of titanium shown in the Fig. 8 two electronic bands of slightly different binding energy from the Fermi level are distinguished. There are two bands: one with completely hybridized orbitals is observed at the energy -0.2 eV, whereas the other which possesses symmetry A_{1g} is observed at the energy -0.4 eV. The filling of the lower band in the partial density of d states of Ti1 atom is remarkably enhanced, as is seen in Fig.8. According to DOS calculations, the contribution from Ti2 atoms should exceed the contribution from Ti1. However, these two contributions of Ti1 and Ti2 in valence band ResPES are observed as one broad peak labelled as Ti_d in Fig. 5 because of the selected energy resolution of the analyzer. Also, this peak represents electronic states of different symmetry. To illustrate, let us consider excitation dynamics of Ti 2p ResPES. At excitation energies from **b)** to **f)** in Ti $L_{2,3}$ XAS in Fig. 5, mainly the t_{2g} states (at octahedral symmetry) are excited, whereas when increasing the excitation energy from **f)** to **i)** the contribution of e_g states is increased. From those considerations Ti_d peak represents a Ti band mixed of t_{2g} and e_g states localized near the Fermi level. A nature of resonance can be easily determined from constant intensity spectra (CIS) which are the intensity profiles of Ti_d and Mn_d peaks plotted in the X-ray absorption energy scale. In Fig.9 Ti_d intensity profile taken at binding energy of 0.2 eV from Ti 2p ResPES and that of Mn_d taken at the energy 0.3 eV from Mn 2p ResPES are shown. As can be seen both Ti_d and Mn_d CIS include all the peculiarities of L_3 XAS of Ti and Mn respectively that indicates a presence of Ti and Mn 3d band located in the vicinity of the Fermi energy. Results of band structure calculations shown in Fig. 7 support this conclusion.

4. Conclusion

For Mn atoms the mixed ionic-covalent chemical bonding in the octahedral surrounding is observed. These results are confirmed by the atomic

multiplet calculations of Ti, Mn XAS and Mn 2p XPS. According to all experimental data electrons are transferred from the manganese ions to the conduction band formed by the Ti 3d states.

In ResPES of the valence band excited at 2p resonance of Ti and Mn correspondingly Ti and Mn bands of mixed orbital symmetry localized just below the Fermi level have been detected. Performed $E(\mathbf{k})$ band structure calculations suggest that Ti 3d states are localized in the vicinity of point Γ of the Brillouin zone of the crystal. The Mn 3d states are localized along the direction $M-\Gamma-K$.

Overall, chemical bonding situation in Mn intercalates is found to be quite outstanding when compared with the cases of other TM intercalates.

5. Acknowledgment

We acknowledge the financial support of the RFBR, grant N 09-03-00053. We are thankful to F. de Groot for the opportunity to use his XAS code, Mikhail Korotin for useful recommendations, Michele Zacchigna for fruitful scientific discussion and Federica Bondino for a help with the beamline instrumentation.

References

- [1] A. Postnikov, M. Neumann, S. Plogmann, Y. Yarmoshenko, A. Titov, A. Kuranov, Computational Materials Science 17 (2000) 450–454.
- [2] A. Titov, A. Kuranov, V. Pleschev, Y. Yarmoshenko, M. Yablonskikh, A. Postnikov, S. Plogmann, M. Neumann, A. Ezhov, E. Kurmaev, Physical Review B - Condensed Matter and Materials Physics 63 (2001) 351061–351068.
- [3] A. Titov, S. Titova, M. Neumann, V. Pleschov, Y. Yarmoshenko, L. Krasavin, A. Kuranov, Molecular Crystals and Liquid Crystals 311 (1998) 161–166.
- [4] A. Titov, A. Dolgoshein, I. Bdikin, S. Titova, Physics of the Solid State 42 (2000) 1610–1612.
- [5] T. V. Kuznetsova, A. N. Titov, Y. M. Yarmoshenko, E. Z. Kurmaev, A. V. Postnikov, V. G. Pleschev, B. Eltner, G. Nicolay, D. Ehm, S. Schmidt, F. Reinert, S. Hufner, Phys. Rev. B 72 (2005) 085418.

- [6] X. Cui, H. Negishi, S. Titova, K. Shimada, A. Ohnishi, M. Higashiguchi, Y. Miura, S. Hino, A. Jahir, A. Titov, H. Bidadi, S. Negishi, H. Namatame, M. Taniguchi, M. Sasaki, *Physical Review B - Condensed Matter and Materials Physics* 73 (2006) 1–6.
- [7] A. Titov, Y. Yarmoshenko, M. Neumann, V. Pleshchev, S. Titova, *Physics of the Solid State* 46 (2004) 1681–1685.
- [8] V. Maksimov, N. Baranov, V. Pleschov, K. Inoue, *Journal of Alloys and Compounds* 384 (2004) 33–38.
- [9] Y. Tazuke, T. Miyashita, H. Nakano, R. Sasaki, *Physica Status Solidi (C) Current Topics in Solid State Physics* 3 (2006) 2787–2790.
- [10] Y. Tazuke, T. Takeyama, *Journal of the Physical Society of Japan* 66 (1997) 827–830.
- [11] M. Zangrando, M. Finazzi, G. Paolucci, G. Comelli, B. Diviacco, R. Walker, D. Cocco, F. Parmigiani, *Review of Scientific Instruments* 72 (2001) 1313–1319.
- [12] P. Blaha, K. Schwarz, G. K. H. Madsen, D. Kvasnicka, J. Luitz, *Wien2k, an augmented plane wave + local orbitals program for calculating crystal properties* (karlheinzh schwarz, techn. universitat wien, austria), 2001.
- [13] J. P. Perdew, K. Burke, M. Ernzerhof, *Physical Review Letters* 77 (2010) 3865–3868.
- [14] E. Stavitski, F. D. Groot, *Micron* 41 (2010) 687–694.
- [15] A. S. Shkvarin, Y. M. Yarmoshenko, N. A. Skorikov, M. V. Yablonskikh, E. G. Shkvarina, A. N. Titov, *Journal of Experimental and Theoretical Physics* 140 (2011).
- [16] A. E. Bocquet, T. Mizokawa, T. Saitoh, H. Namatame, A. Fujimori, *Physical Review B - Condensed Matter and Materials Physics* 46 (1992) 3771–3784.
- [17] A. Fujimori, S. Suga, H. Negishi, M. Inoue, *Phys. Rev. B* 38 (1988) 3676–3689.

- [18] A. N. Titov, Y. M. Yarmoshenko, M. Neumann, V. G. Pleshchev, S. G. Titova, *Physics of the Solid State* 46 (2004) 1681–1685.
- [19] A. N. Titov, Y. M. Yarmoshenko, A. Zimina, M. Yablonskikh, A. V. Postnikov, S. Eisebitt, *Physics of the Solid State* 50 (2008) 1186–1190.
- [20] S. Bayliss, W. Liang, *Journal of Physics C: Solid State Physics* 17 (1984) 2193–2201.
- [21] F. Gamble, *Journal of Solid State Chemistry* 9 (1974) 358–367.
- [22] D. W. Bullett, *Journal Physics C : Solid State Physics*. 11 (1978) 4501–4515.
- [23] R. Huisman, R. de Jonge, C. Haas, F. Jellinek, *Journal of Solid State Chemistry* 3 (1971) 56–66.
- [24] C. Sugiura, S. Shoji, S. Kojima, *Japanese Journal of Applied Physics, Part 1: Regular Papers and Short Notes and Review Papers* 30 (1991) 1742–1745.
- [25] J. W. Allen, *Synchrotron Radiation Research*, volume 25, Plenum Press, N.Y., 1992.
- [26] A. Kay, E. Arenholz, S. Mun, F. G. D. Abajo, C. Fadley, R. Denecke, Z. Hussain, M. V. Hove, *Science* 281 (1998) 679–683.
- [27] J.-E. Rubensson, J. Luning, S. Eisebitt, W. Eberhardt, *Applied Physics A: Materials Science and Processing* 65 (1997) 1742–1745.
- [28] N. Mårtensson, M. Weinelt, O. Karis, M. Magnuson, N. Wassdahl, A. Nilsson, J. Stöhr, M. Samant, *Applied Physics A: Materials Science and Processing* 65 (1997) 159–167.
- [29] G. Armen, H. Wang, *Physical Review A* 51 (1995) 1241–1247.
- [30] C. Powell, A. Jablonski, *Journal of Physical and Chemical Reference Data* 28 (1999) 19–62.
- [31] J. Yeh, I. Lindau, *Atomic Data and Nuclear Data Tables* 32 (1985) 1–155.

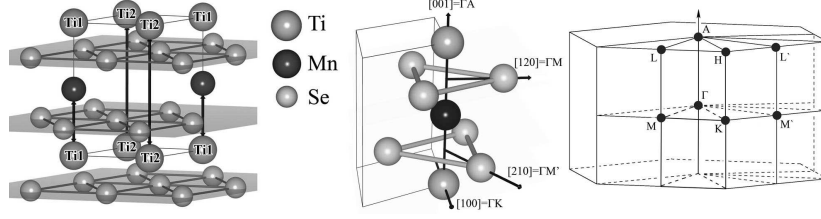


Figure 1: A fragment of the $\text{Mn}_{0.2}\text{TiSe}_2$ crystal and Brillouin zone for the 1T- TiSe_2 compound. Γ -A direction in the Brillouin zone corresponds to the direction of the crystallographic (c)-axis perpendicular to the basic plane of the crystal in the direct space ($[001]$ direction).

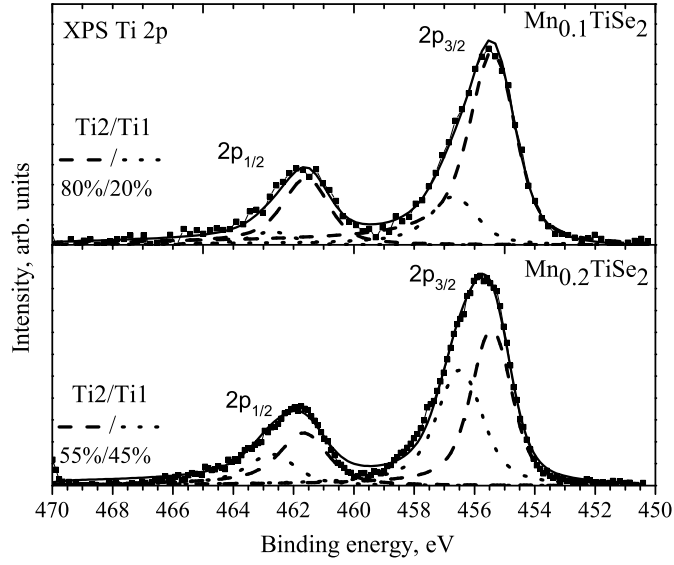


Figure 2: XPS of Ti 2p core levels in Mn_xTiSe_2 ($x=0.1$ and 0.2) and their fit are presented. Spectral contributions of Ti2 and Ti1 atoms are shown by a long dash line and short dash line respectively at both top and bottom frames of the graph. Corresponding Ti2/Ti1 ratio numbers are given.

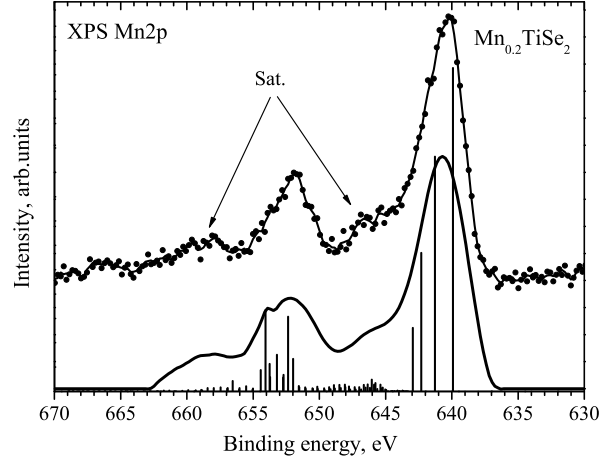


Figure 3: Mn 2p X-ray Photoelectron spectrum of $\text{Mn}_{0.2}\text{TiSe}_2$. Positions of the satellites are marked with the label "Sat." Calculated XPS is shown at the bottom part of the graph.

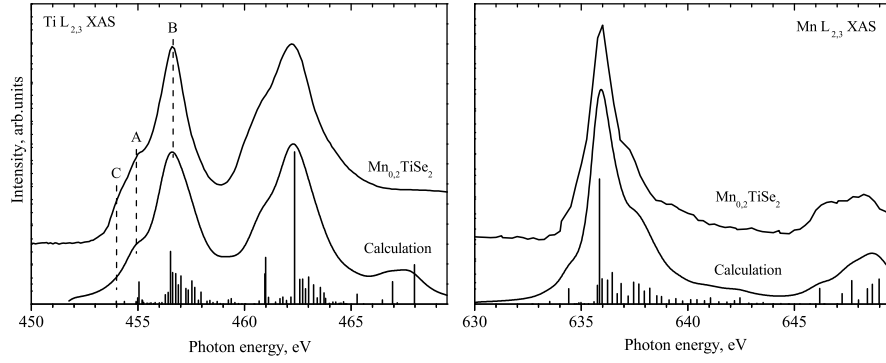


Figure 4: Experimental (top) and calculated (bottom) Ti $L_{3,2}$ and Mn $L_{3,2}$ X-ray Absorption Spectra of $\text{Mn}_{0.2}\text{TiSe}_2$.

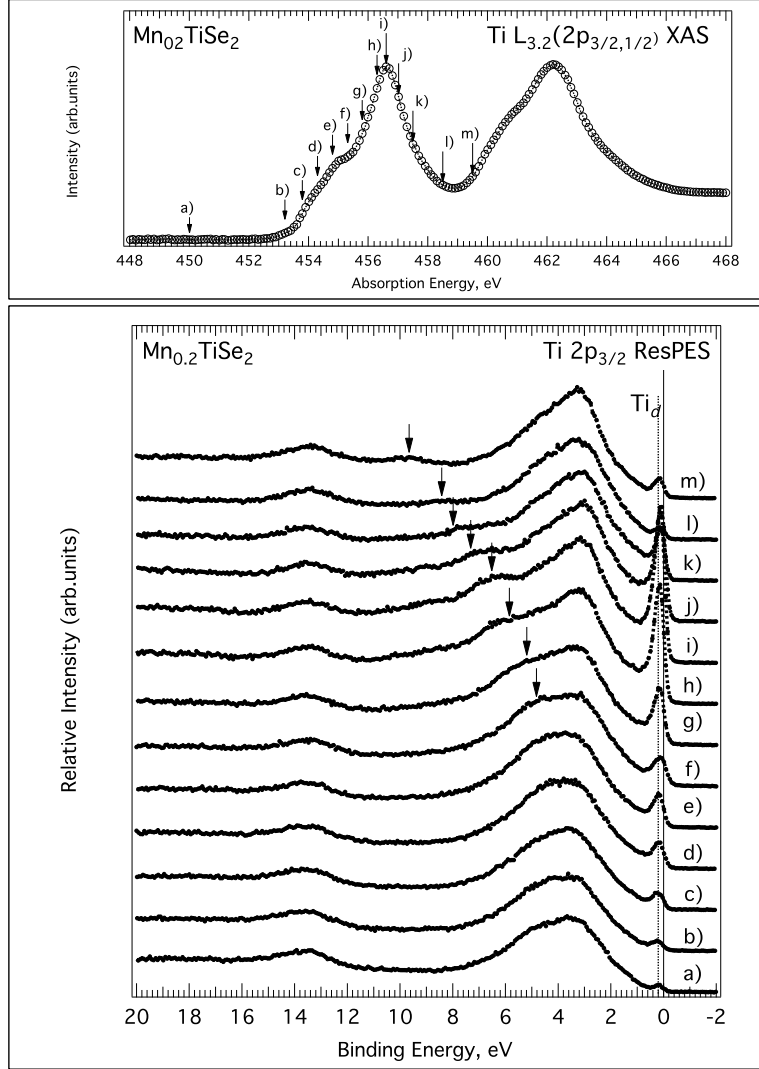


Figure 5: Ti 2p valence band Resonant Photoemission Spectra (ResPES) of $Mn_{0.2}TiSe_2$. At the top frame Ti $L_{3,2}$ X-ray absorption spectrum is shown. Excitation energies are labelled by down arrows in XAS and marked with letters from a) to m). In the bottom frame, corresponding ResPES are labelled accordingly. Down arrows in the bottom frame mark positions of the Auger contribution. Peak with the binding energy 13.5 eV corresponds to Se 4s band.

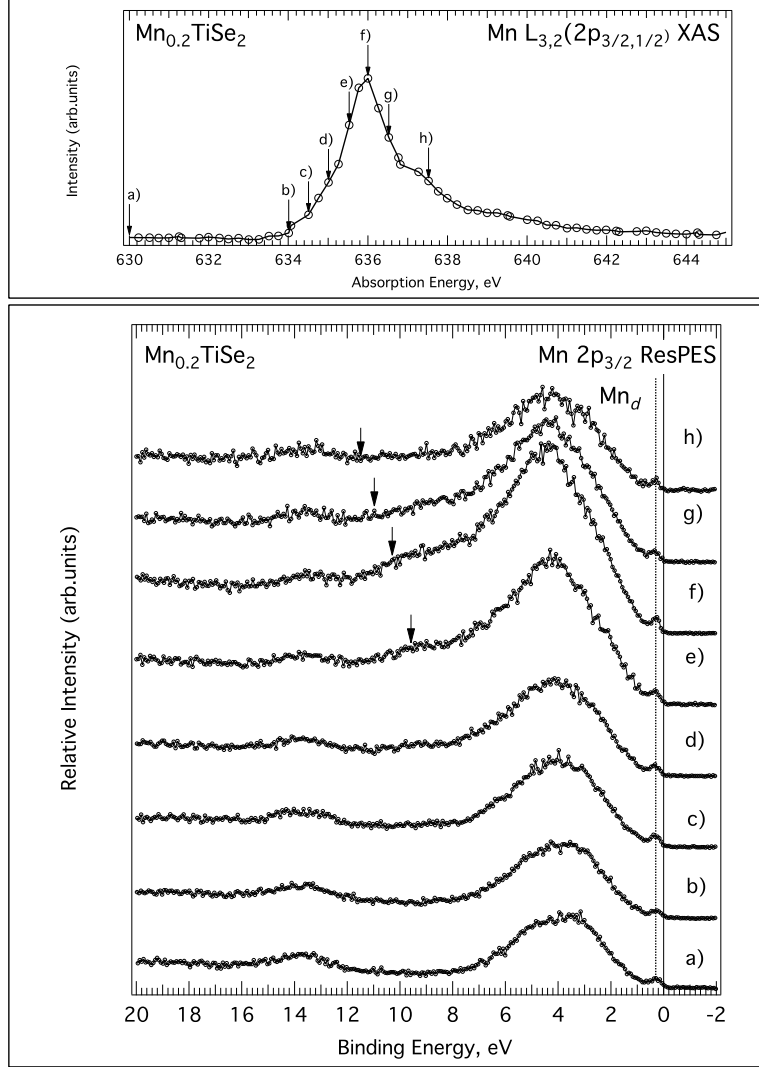


Figure 6: Mn 2p valence band Resonant Photoemission Spectra of $\text{Mn}_{0.2}\text{TiSe}_2$. All designations are the same as in Fig. 5.

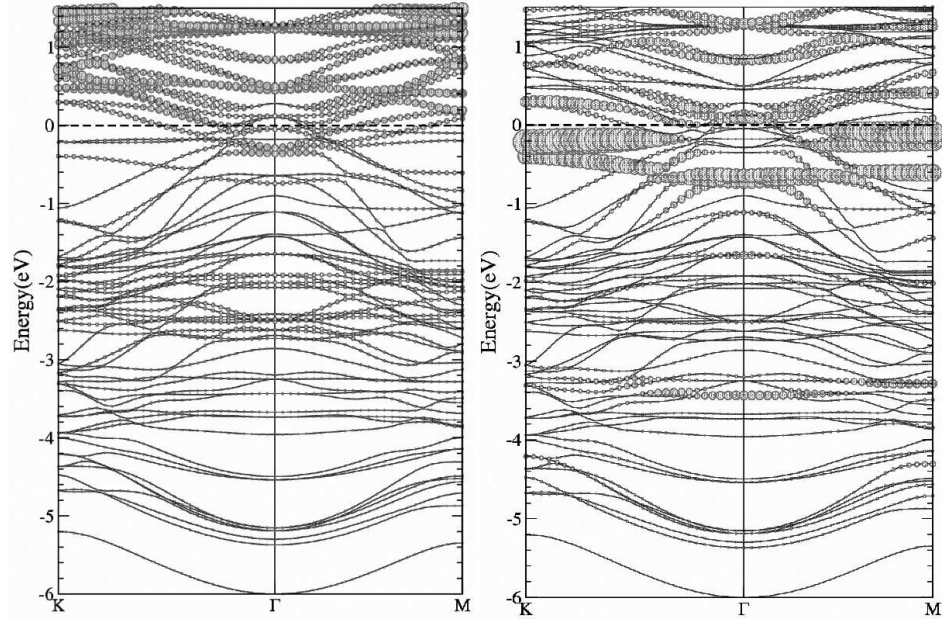


Figure 7: Calculated dispersion curves for $\text{Mn}_{1/8}\text{TiSe}_2$, the circle diameter is proportional to the 3d zone filling by the titanium states (left panel) and manganese states (right panel). Under the Fermi level the 3d states of titanium picked out in the vicinity of point Γ mainly possess the mixed E_g^σ , E_g^π and A_{1g} orbital symmetry (energy 0.2 eV) . The Mn 3d states in directions $K - \Gamma - M$ occupy the energy range from the Fermi level up to 0.5 eV. They are also possess mixed E_g^σ , E_g^π and A_{1g} e_g - t_{2g} orbital symmetry.

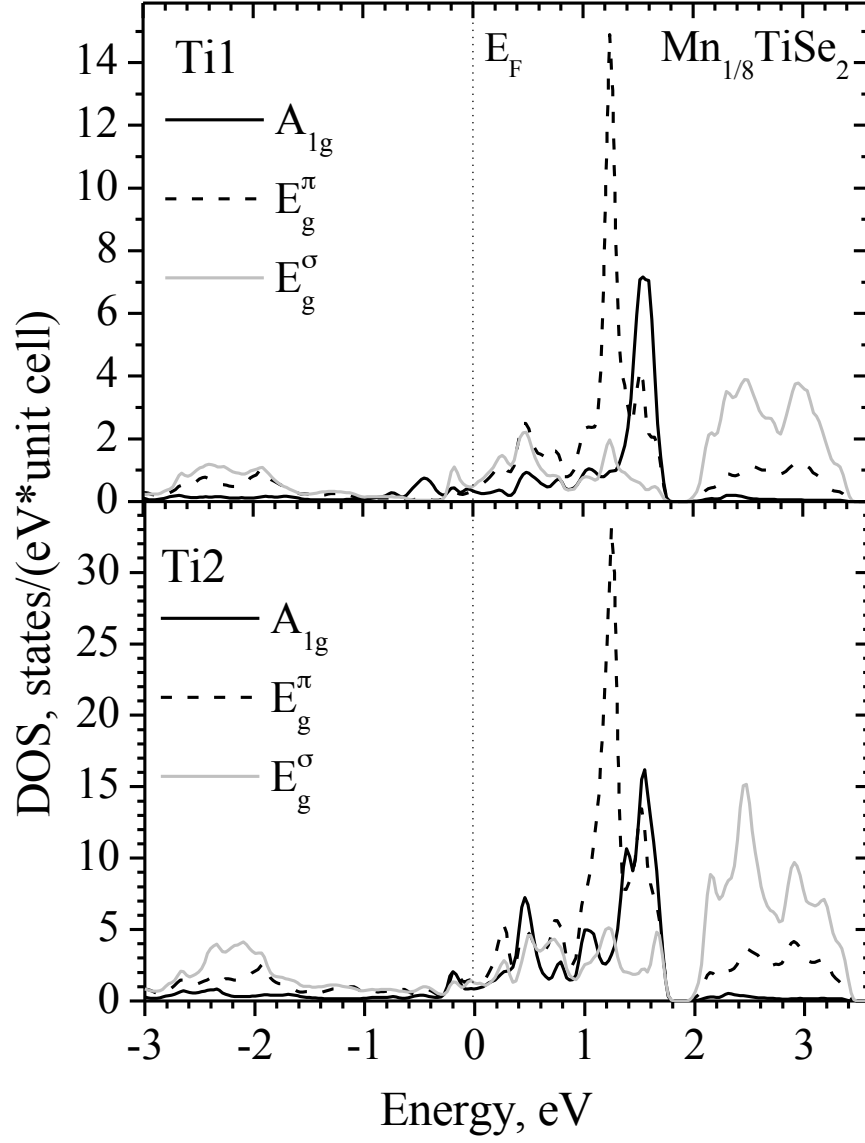


Figure 8: Local density of states Ti 3d in two nonequivalent positions Ti1 and Ti2. For Ti1 a relative increase of the A_{1g} contribution to the states under the Fermi level in the energy range 0.2-0.3 eV is observed. Partial densities of states are given per formula unit.

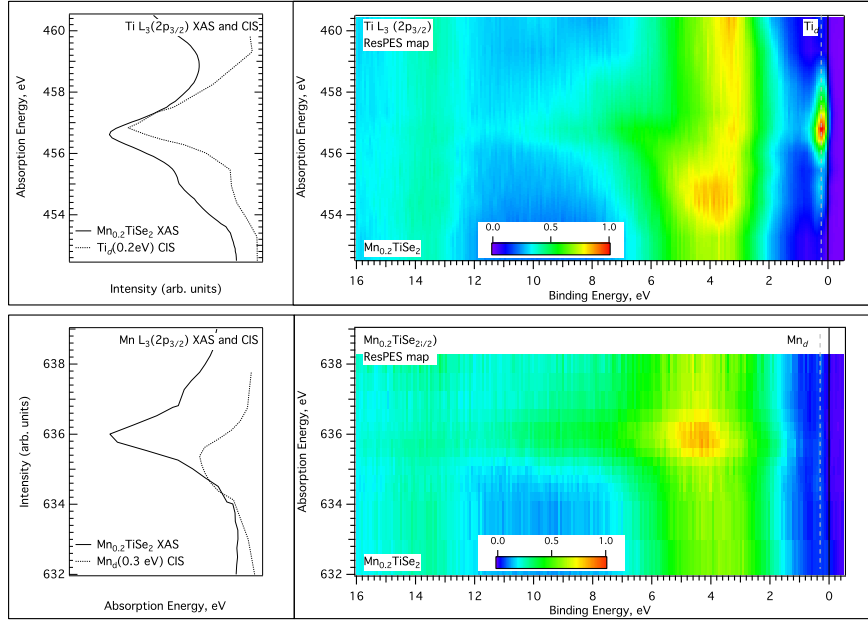


Figure 9: XAS, CIS (at the left side of the graph) and relative intensity maps of Ti and Mn 2p ResPES interpolated out of data shown in Figs 5,6 (right side of the graph). At the top line the case of Ti excitation is presented. At the bottom line the case of Mn excitation is displayed. At the left side of the graph, X-ray absorption and constant intensity spectra are shown with solid and dotted lines respectively. At the right side of the graph, a position of an intensity profile in the binding energy scale is marked with a dotted line.